JOURNAL OF GEOPHYSICAL RESEARCH: SPACE PHYSICS, VOL. 118, 3995–4004, doi:10.1002/jgra.50398, 2013

Magnetic correlation functions in the slow and fast solar wind in the Eulerian reference frame

James M. Weygand,[1,2] W. H. Matthaeus,[3] M. G. Kivelson,[1,2] and S. Dasso[4]

Received 18 January 2013; revised 28 May 2013; accepted 15 June 2013; published 24 July 2013.

[1] Simultaneous multiple point measurements of the magnetic field from seven spacecraft are employed to estimate the Eulerian correlation function and decorrelation time scales in the near Earth solar wind for two different solar wind speed ranges. We find that the Eulerian decorrelation time scale differs significantly in the slow solar wind (<450 km/s), where quasi-two-dimensional turbulence dominates, and in the fast solar (>600 km/s) wind, where slab-type turbulence dominates. In slow solar wind, the decorrelation time is 215 ± 43 min, and in fast solar wind, the decorrelation time scale is 114 ± 23 min, which indicates that decorrelation times vary with the nature of the turbulence. The values reported here are comparable to estimates of decorrelation times based on a number of different models, but do not clearly support or refute any specific solar wind turbulence model. These results may be useful in magnetohydrodynamic modeling of the solar wind and can contribute to our understanding of solar and galactic cosmic ray diffusion in the heliosphere.

Citation: Weygand, J. M., W. H. Matthaeus, M. G. Kivelson, and S. Dasso (2013), Magnetic correlation functions in the slow and fast solar wind in the Eulerian reference frame, *J. Geophys. Res. Space Physics*, *118*, 3995–4004, doi:10.1002/jgra.50398.

1. Introduction

[2] Most single-spacecraft studies of the solar wind have assumed that the flow and magnetic field fluctuations in the solar wind are frozen in and do not evolve much over time scales [*Taylor*, 1938] on the order of the travel time from the L1 point to the Earth's magnetosphere, i.e., times of order 1 h. Comparisons of spacecraft data obtained at the L1 and data recorded just outside the Earth's bow shock show this assumption is relatively reliable [*Paularena et al*., 1999; *Ridley*, 2000]. However, the time scale over which the frozen-in flow assumption remains valid has not been fully established. Furthermore, the rate of decorrelation in the plasma frame, which is the principal contributor to the violation of the frozen-in assumption, is a fundamental property of the dynamics of the turbulence. Understanding this decorrelation would provide important insights into plasma turbulence theory.

[3] A useful development in the study of time decorrelations was the introduction of a method [*Dasso et al*., 2008; *Matthaeus et al*., 2010] to formulate a leading order estimate of the rate of decorrelation in the Eulerian frame, by comparison of single-spacecraft and multiple-spacecraft analyses. *Dasso et al*. [2008] examined a single day of magnetic field data from ACE and Wind in which the solar wind had an average speed of about 450 km s^{-1}. From the *Dasso et al*. [2008] analysis, one derives a decorrelation value of about 3 h. The method was subsequently applied to a decade of magnetic field data obtained by the ACE and Wind spacecraft at times when the separation vector was within 30 degrees of the average solar wind flow vector [*Matthaeus et al*., 2010]. This more complete study concluded that the magnetic field fluctuations decorrelate over time scales of 2.9 h. These studies demonstrate that over longer time intervals, the frozen-in approximation is not expected to apply, and the turbulence must be viewed not as static but as a highly dynamic medium.

[4] *Matthaeus et al*. [2010] estimated the Eulerian decorrelation function by comparing two-spacecraft spatial correlations with single-spacecraft time-lagged correlations. The two-spacecraft spatial correlations (called "two-point correlations" below) were obtained using simultaneous data, averaging over a period of 24 h. These two-point spatial correlations are assumed to come from turbulent magnetic field fluctuations. For the single-spacecraft temporal correlations ("single-point correlations"), the temporal separations were determined from the mean spacecraft separation divided by the mean solar wind speed over a 24 h interval. The method for obtaining the Eulerian decorrelation relies on the assumption that the single-point correlations differ from the two-point correlations because they incorporate additional decorrelation effects associated with the passage of time between the lagged single-point measurements—that is, the temporal decorrelation is related to departures from the Taylor frozen-in approximation.

[1]Institute of Geophysics and Planetary Physics, University of California, Los Angeles, California, USA.
[2]Department of Earth and Space Science, University of California, Los Angeles, California, USA.
[3]Bartol Research Institute and Department of Physics and Astronomy, University of Delaware, Newark, Delaware, USA.
[4]Departamento de Física (FCEN-UBA), Instituto de Astronomía y Física del Espacio (UBA, CONICET), Buenos Aires, Argentina.

Corresponding author: J. M. Weygand, Institute of Geophysics and Planetary Physics, University of California, Los Angeles, CA 90095-1567, USA. (jweygand@igpp.ucla.edu)

2169-9380/13/10.1002/jgra.50398

[5] This earlier study grouped all the available data together and did not sort the sample population by solar wind speed. However, it is generally accepted that the magnetic field fluctuations associated with turbulence display different characteristics in the slow and fast solar wind [*Goldstein et al*., 1994; 1995; *Weygand et al*., 2011]. The present paper examines whether Eulerian decorrelation occurs at different rates in these two types of solar wind.

[6] Prominent among the known differences in fast and slow wind properties is a variation in "turbulence geometry" that has been characterized as a varying admixture of slab and quasi-two-dimensional (2D) turbulence [*Dasso et al*., 2005]. The slab-2D parameterization is based on the relative power in quasi-slab, spectral fluctuations, and low-frequency quasi-two-dimensional fluctuations. *Ruiz et al*. [2011] have shown that the varying mixture of the slab and 2D turbulence is related to the progressive dynamic spectral transfer of energy from "slab" modes to "2D" modes as the solar wind parcels age from younger to older. The use of slab-2D parameterization is convenient in cosmic ray scattering and observational studies [*Bieber et al*., 1994; *Bieber et al*., 1996] and characterizes the anisotropy that emerges naturally in the theory of low Mach number nearly incompressible magnetohydrodynamics (MHD) [*Zank and Matthaeus*, 1992]. From a theoretical perspective, variation in slab-2D ratio reflects changes in the balance of physical effects that drive the dynamics and induce time decorrelation.

[7] Beyond the assumption of any particular model, it is well known that the turbulence geometry, that is, the distribution of energy over angles of wave vectors measured relative to the mean magnetic field, is a major factor in determining the correlation time scales of MHD turbulence [*Montgomery*, 1982; *Zhou et al*., 2004; *Servidio et al*., 2011]. Mainly motivated by charged particle scattering theory, the two-component slab-2D representation has been employed as a basis for modeling the inertial range MHD time decorrelations [*Bieber et al*., 1994; *Shalchi et al*., 2006]. If one further extends the modeling by adopting a specific form for the energy spectrum, then one can construct models for the entire Eulerian single-point, two-time correlation function [*Shalchi*, 2008]. Regardless of whether these explicit models are accurate (see below), the assembly of such models demonstrates how different spectral characteristics may influence the Eulerian correlation. In particular, the orientation of the wave vector induces variations in the Alfvén time scale, while the magnitude of the wave vector influences both the nonlinear time scale and the Alfvén time scale. Adding contributions from all parts of the spectrum results in the total observed time decorrelation. The slow wind is found to contain more quasi-two-dimensional turbulence while the fast wind contains relatively more slablike turbulence. Furthermore, fast solar wind and slow solar wind have different correlation scale lengths [*Weygand et al*., 2011]. As we will see in more detail below, these factors lead us to expect that time decorrelation will differ in the two classes of solar wind [*Shalchi et al*., 2006; *Shalchi*, 2008].

[8] In this study, we separate the solar wind into two different types: slow (< 450 km/s) and fast (> 600 km/s) solar wind in order to establish the Eulerian correlation function for each speed range. We adopt the method used by *Matthaeus et al*. [2010] to estimate the Eulerian correlation function. This enables us to examine the validity of the frozen-in assumption for both the slow and fast solar wind. The main conclusion will be that the estimates of the average decorrelation time differ in fast wind and slow wind samples. In section 2, we discuss the spacecraft data used in this study, and in section 3, we describe the procedure used to analyze data and to obtain the empirical Eulerian correlation functions. In section 4, we interpret the results and discuss theoretical issues that arise in view of the observed differences in Eulerian correlations in fast and slow solar wind.

2. Instrumentation

[9] This study makes use of the magnetic field measurements taken within the solar wind by instruments on many different spacecraft, including ACE, Geotail, IMP 8, Interball, THEMIS/ARTEMIS, and Wind. This collection provides simultaneous two-point plasma and field measurements at a large range of spatial separations, enabling measurement of spatial correlations as a function of separation directly instead of inferring them by interpreting temporal fluctuations as frozen into a flowing plasma [*Taylor*, 1938; *Jokipii*, 1973]. Magnetic field and plasma data from the THEMIS/ARTEMIS mission are restricted to the P1 and P2 spacecraft in this study. From approximately mid June to mid October from 2007 to 2009, the apogees align on the dayside of the magnetosphere and provide data from spacecraft separations on the order of 10 R_E. In mid 2009, the orbits of the THEMIS/ARTEMIS P1 and P2 spacecraft were altered in order to insert them into orbit around the Moon for future lunar studies, and the two spacecraft were renamed P1 and P2, respectively. This change in the orbits provides additional spacecraft separations ranging from 10 to 30 R_E.

[10] Each THEMIS/ARTEMIS spacecraft carries a boom-mounted triaxial fluxgate magnetometer (FGM) [*Auster et al*., 2008] and an electrostatic analyzer (ESA) [*McFadden et al*., 2008]. Magnetic field vectors routinely are available at 64 Hz resolution (nominal mode). Both preflight and in-flight calibrations of the two magnetometers have been performed. The relative uncertainty in the data after calibration is at most 0.1 nT, an estimate determined by examining the drift in the offset after calibration (H. Schwarzl, private communication, 2010). The digital resolution of the magnetometer is on the order of 0.01 nT [*Auster et al*., 2008]. Data from the ESA plasma instrument provide fundamental plasma parameters such as density, velocity vectors, the pressure tensor, and heat flux. The uncertainties in most of these quantities are not significant for this study, and only the general identification of the solar wind is important.

[11] In addition to THEMIS/ARTEMIS data, we also use solar wind data from the ACE, Geotail, IMP 8, Interball, and Wind spacecraft. On all five of these spacecraft, we use data from triaxial fluxgate magnetometers [*Smith et al*., 1998; *Kokubun et al*., 1994; *Nozdrachev et al*., 1995; *Lepping et al*., 1995] to obtain the local interplanetary magnetic field direction and magnitude at temporal resolution ranging from 3 s to 16 s, with an uncertainty of about 0.3 nT associated with the IMP 8 data and uncertainties on the order of 0.1 nT for the other four. Magnetic field data from ACE were provided at 16 s resolution, Geotail and Wind data were at 3 s resolution, IMP 8 data were at 15 s resolution, and Interball data were at 6 s resolution.

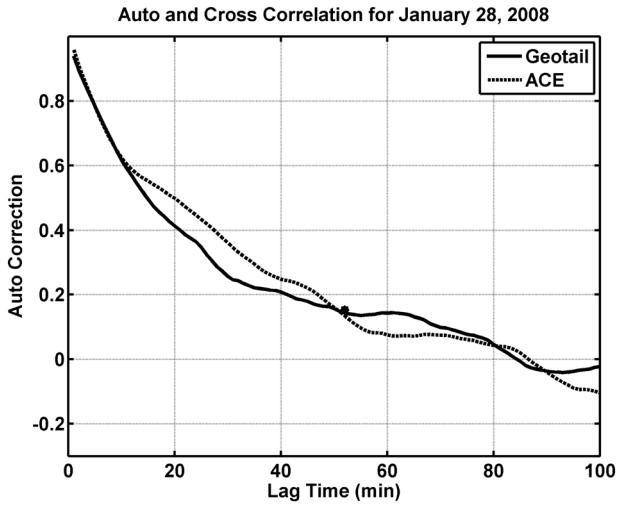

Figure 1. Single-point and two-point correlations for interplanetary magnetic field data from 28 January 2008 starting at 2000 UT and lasting 12 h. The solid curve is the single-point correlation curve for the Geotail magnetic field for time lags from 1 to 100 min. The dotted line is the single-point correlation curve for the ACE magnetic field. The asterisk (*) represents the two-point correlation value between the two spacecraft and is plotted at time t_i, the transit time between the spacecraft at the mean solar wind speed. Note that the frozen-in flow estimate of the single-point correlation falls lower than the two-point correlation.

3. Procedure and Observations

[12] The first step is to select intervals that can be confidently identified as being within the solar wind. The THEMIS/ARTEMIS solar wind data intervals are selected visually from plotted data by excluding data at or within the bow shock. The solar wind is identified from both the magnetic field and the plasma measurements. The magnetic field magnitude is expected to be on the order of several nanoteslas and relatively smooth with respect to the high-frequency, large-amplitude (~10 nT) fluctuations associated with the bow shock. The solar wind plasma is required to be greater than or equal to 250 km s^{-1}, the ion energy flux had to show a beam of ion energy fluxes at about 1 keV, and the plasma density is expected to be greater than 1 particle per cm^{-3}. The choice of 250 km s^{-1} as a cutoff velocity, although arbitrary, excludes magnetosheath data. We also limit our observations to local times within a few hours of noon to avoid including intervals from regions of high-speed flows within the magnetosheath that may be present on the flanks of the magnetosphere. We do not use solar wind data with sharp rotations in the B_x and B_y GSE components in order to exclude sector boundary crossings. We remove solar wind shocks and other discrete solar wind structures associated with sharp gradients in the flow speed, density, and total magnetic field that occur over a time range of a few minutes. The THEMIS/ARTEMIS P1 and P2 spacecraft remain relatively close together (<25 R_E) and are used to characterize fluctuations over short distances. We exclude intervals within the solar wind of less than 1 h for analysis of these short spatial separations. The THEMIS/ARTEMIS orbits remain in relatively close proximity to the bow shock, even when in the solar wind. Inevitably, foreshock waves are present in some of the selected intervals. To minimize the contribution of such waves to the analysis, the solar wind magnetic field measurements are averaged to 30 s resolution, which is approximately the longest period for ion foreshock waves.

[13] We define slow solar wind as $\leq$450 km s^{-1} and fast solar wind as $\geq$600 km s^{-1} for this study. In order to obtain two-point correlation coefficients at larger separations, we require longer continuous intervals for analysis. Therefore, for the larger separations, we use only intervals with more than 12 h of continuous data at 1 min resolution for slow solar wind intervals and more than 8 h of continuous data at 1 min resolution for fast solar wind intervals. These interval lengths are chosen to maximize the number of useful intervals while maintaining enough data points in each interval to provide stable two-point correlation values.

[14] Data from the ACE, Geotail, IMP 8, Interball, and Wind spacecraft yield two-point correlations at larger separations, and the pair of THEMIS/ARTEMIS spacecraft provide smaller separations. We linearly interpolate the data from each spacecraft to 1 min resolution, obtaining, in effect, simultaneous field vectors at the spacecraft position because the sampling rate varied from spacecraft to spacecraft. For the ACE, Geotail, Wind, IMP 8, and Interball spacecraft, solar wind intervals could be identified by an automated procedure because of their nearly continuous immersion within the solar wind. For the THEMIS/ARTEMIS spacecraft closer to the magnetosphere, we selected the intervals by eye to assure that no magnetosheath values crept into our study. The long life time of many of the spacecraft missions and the continuity of the field and plasma data over long intervals provided thousands of intervals for this study.

[15] Since we are interested in the Eulerian frame (the zero mean momentum frame, i.e., the frame moving with the solar wind), we subset our solar wind data to intervals for which the mean solar wind velocity lies within 30° of the mean spacecraft separation vector of a pair of spacecraft. In this subset of intervals, we assume that the same parcel of solar wind sweeps past both nearly aligned spacecraft, enabling us to determine how much a parcel of solar wind has evolved in the time to flow from one spacecraft to the other. From the available data, we found 2570 intervals meeting our restrictions, including 1076 slow solar wind intervals and 662 fast solar wind intervals. The remaining 832 intervals were linked to intermediate solar wind speeds between 450 km s^{-1} and 600 km s^{-1}.

[16] From each interval, we obtain one estimate of the two-spacecraft correlation and two estimates of single-point correlation values (one for each spacecraft). The single-point correlation values are determined by time-lagging the data from a single spacecraft. The single-point correlation of interest to our study is found by setting the time lag to the interspacecraft transit time t_i (i.e., the time to pass from the upstream spacecraft to the downstream spacecraft at the computed mean solar wind speed).

[17] Figure 1 shows the single-point correlation function for Geotail (solid curve) at (21, 1.3, –4.5) R_e GSE and ACE (dashed curve) at (220, 26, 15) R_e GSE for one of the selected solar wind intervals on 28 January 2008 starting at 2000 UT and lasting 12 h. The angle between the flow vector and the spacecraft separation vector is ~10.5°. The asterisk (*) plotted at the interspacecraft transit time $t_i = 51.9$ min indicates

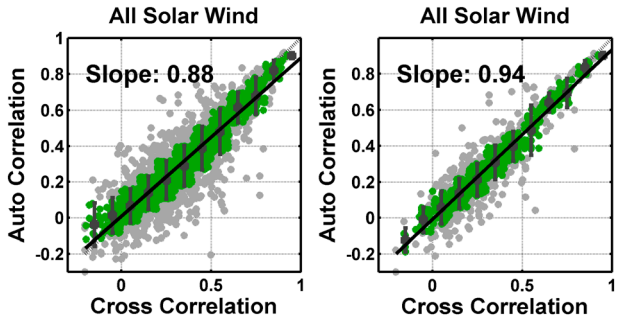

Figure 2. Scatter plot of the single-spacecraft correlation (Rssc) versus two-spacecraft correlation (Rmsc) from ACE, Wind, Geotail, IMP-8, and THEMIS/ARTEMIS P1 and P2 pairs for all solar wind speeds. The single-point correlation is evaluated at a time lag computed as the transit time between spacecraft at the mean solar wind speed. The dotted line has a slope of 1. The solid line is a least squares fit to the means (squares) of 0.1 wide bins, and the bars are the standard deviation within each bin. The green points are those within one standard deviation of the mean. The slope of the fit is given in the upper left corner. The angle between the spacecraft separation vector and solar wind flow vector was allowed to be as large as 30° for the data points in the left panel and 10° for the data points in the right panel.

the two-point correlation value (0.15) for the ACE and Wind magnetic field vectors. The single-point correlations for Geotail and ACE at time t_i are 0.14 and 0.13, respectively. The assumption is that the time evolution during the transit time between the spacecraft positions is the dominant factor in producing the difference between the single-point correlation and two-point correlation values [*Matthaeus et al*., 2010].

[18] From a large set of single- and two-point correlation values evaluated without restriction of the solar wind velocity, we find a significant spread in a plot of single-point correlations versus two-point correlations, as shown in the left panel of Figure 2. In the left panel, the mean solar wind velocity lies within 30° of the mean spacecraft separation vector of a pair of spacecraft. The circles are values for the individual intervals, the black squares indicate the means computed in bins of width 0.1, and bars indicate the standard deviation within each bin. Points within one standard deviation of the mean are colored green, and the solid line is a least squares fit to the means of the bins. The slope of the line (0.88) shows that, on average, the two-point correlations are larger than the corresponding auto correlations. Misalignment between the spacecraft separation vector and the flow vector contributes significantly both to the magnitude of the slope and the deviation of the measured points from the linear fit. If we plot data only from intervals when the separation vectors lie within 10° of the flow vector (see the right panel of Figure 2), the slope becomes 0.94 and the standard deviations decrease in most bins. On the other hand, if we include all angles, the slope of the least squares fit drops to 0.78.

[19] Using the single- and two-point correlation values from the left panel of Figure 2, we can obtain the Eulerian correlation values and, from those values, the Eulerian correlation function. The top panel of Figure 3 gives the Eulerian correlation values, defined as Rssc/Rmsc, which is the ratio of the single-spacecraft correlation to the two-point correlation of the spacecraft pair, plotted in gray as a function of time lag. The Eulerian correlation values were determined from only the correlation values within one standard deviation of the mean of the bins in the left panel of Figure 2. We remind the reader that the time lag used is the separation distance between the two spacecraft divided by the mean solar wind speed for each interval. The plus symbols in the top panel are the mean Eulerian correlation value for bins that are 3 min wide, and the error of the mean is plotted for each bin. When the mean Eulerian correlations were initially calculated, some very large values of Rssc/Rmsc were found, corresponding to intervals when the two-point correlation (Rmsc) values are close to zero. Eulerian correlation values greater than 5 and less than –5 have been removed to prevent biases in the mean bin values. The range of ±5 was arbitrarily selected. The black curve in the top panel of Figure 3 is an exponential fit to the means, and the decorrelation time associated with the exponential fit is 226 ± 18 min. An exponential fit was used here because this form has been the convention [*Zhou et al*., 2004; *Shalchi* 2008; *Matthaeus et al*., 2010; *Weygand et al*., 2011] for decorrelation depending on a single time scale, even though the temporal separations do not extend to the decorrelation time. The decorrelation time does not change significantly if we fit the individual ratios rather than the means of the bins. The bottom panel of Figure 3 shows the number of intervals in each bin. We have cut the figure off at lag times of 60 min because there are few additional data at longer lag times.

[20] By analyzing the solar wind without regard to its speed, we are able to compare our results with those of *Matthaeus et al*. [2010]. Figures 2 and 3 are similar to their Figures 3 and 4, even though we have used different and

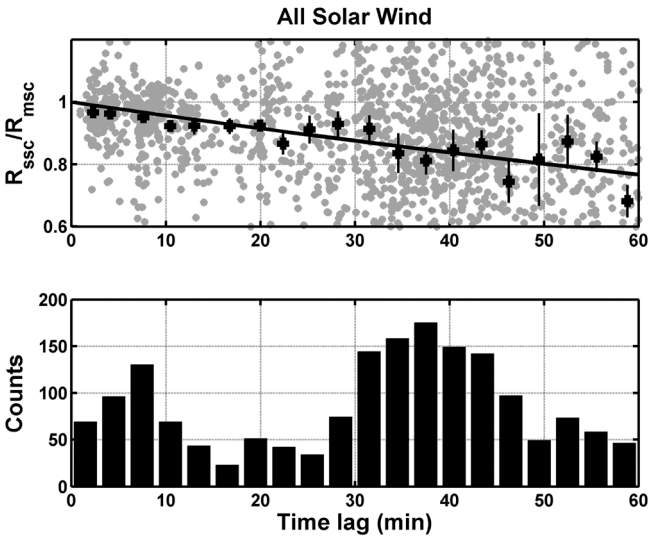

Figure 3. All data: (top) Estimate of the Eulerian correlation function (Rssc/Rmsc) versus the time lag for all values of solar wind speed. The gray symbols are the individual Eulerian correlation values. The black curve is an exponential fit to the binned means of the data (black squares). Bins are 3 min wide, and the black vertical bars are the error of the mean for each bin. The exponential decorrelation time for this fit is 226 ± 18 min. The bottom panel indicates the number of intervals per bin.

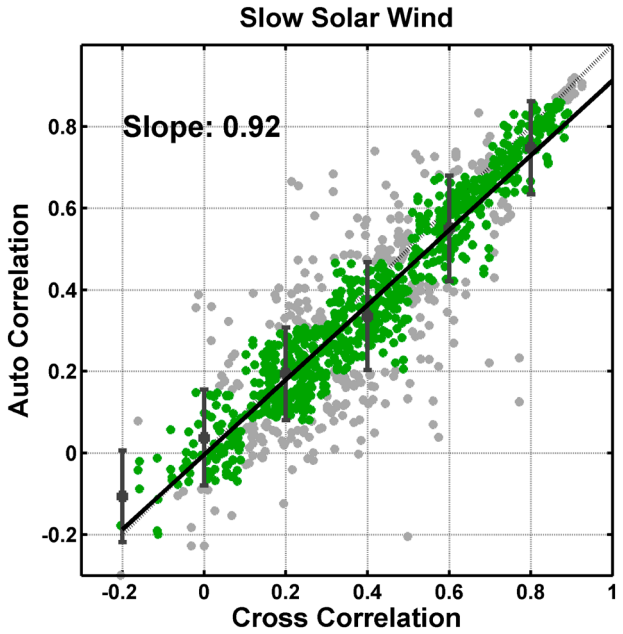

Figure 4. As in Figure 2 but for slow solar wind: (<450 km s^{-1}). Here the bins are 0.2 wide. The angle between the spacecraft separation vector and solar wind flow vector was allowed to be as large as 30° for the data points in this figure.

more time intervals and have included additional spacecraft pairs. Our Figure 2, just like the results of Figure 3 in the *Matthaeus et al*., 2010 study, shows that the average time-lagged single-spacecraft correlation is less than the corresponding two-spacecraft correlation at a fixed spatial lag. The top panel of our Figure 3 displays the ratio of the single-spacecraft correlation to two-point correlation. The ratio of these correlations was fitted with an exponential decay in time lag. The characteristic (*e*-folding) time scale of 226 ± 18 min provides a leading order estimate of the Eulerian decorrelation time and is not dissimilar from the value of 174 min given by *Matthaeus et al*. [2010] obtained from their Figure 4.

[21] In the next two subsections, we carry out a similar analysis in which we further subdivide the data into slow solar wind (≤450 km s^{-1}) and fast solar wind (≥600 km s^{-1}). This will establish whether the characteristic time scale in the Eulerian correlation function varies for different ranges of solar wind velocity.

3.1. Observations

[22] In the next two sections, we bin our solar wind intervals into the slow (≤450 km s^{-1}) and fast (≥600 km s^{-1}) solar wind and repeat the analysis done for the undifferentiated solar wind as discussed above.

3.1.1. Observations: Slow Solar Wind (≤450 km s^{-1})

[23] Figure 4 is analogous to Figure 2 but includes only slow solar wind values. The mean values shown (black squares) are for bins 0.2 wide. The larger range was adopted because there are fewer data available for this scatterplot. The slope of the least squares linear fit, given in the upper left corner (0.92), is larger than that in the left panel of Figure 2, and we used the same range of angles between the spacecraft separation vector and solar wind flow vector (i.e., 30°) as used for the left panel of Figure 2.

[24] The top panel of Figure 5 shows the Eulerian correlation function obtained from the slow solar wind single-point correlation and two-point correlation values. The means shown (black squares) are for 6 min wide bins, and the vertical bars are the errors of the means. For the slow solar wind, the decorrelation time is 215 ± 43 min. This decorrelation time is the same, within the computed uncertainty, as the decorrelation time found using all solar wind speeds. The lower panel of Figure 5 indicates the number of intervals that went into the determination of the Eulerian correlation function.

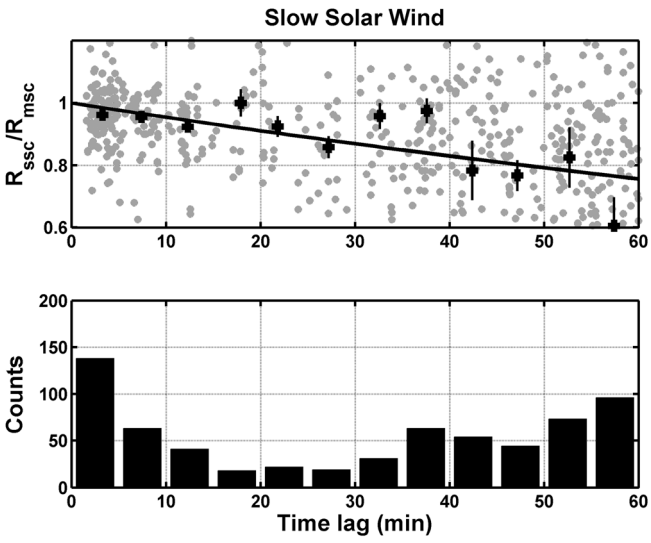

Figure 5. As in Figure 3 but for slow solar wind. Here time lag bins are 6 min wide. The decorrelation time determined from the exponential fit is 215 ± 43.

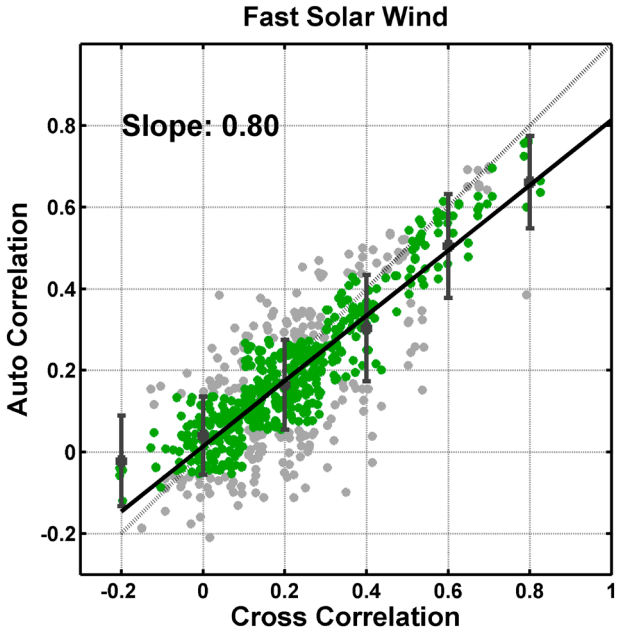

Figure 6. As in Figures 2 and 4 but for fast solar wind (>600 km/s). The time lag bins are 0.2 wide.

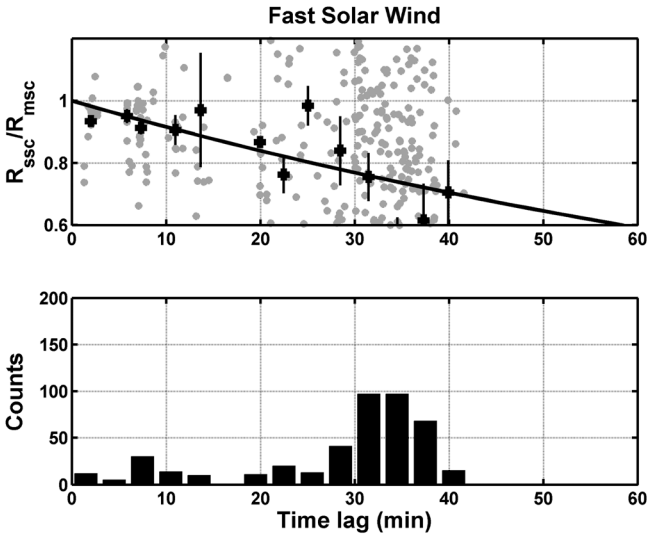

Figure 7. As in Figures 3 and 5 but for fast solar wind. Time lag bins are 6 min wide. The decorrelation time determined from the exponential fit in the bottom panel is 114 ± 23 min.

3.1.2. Observations: Fast Solar Wind (≥600 km s^{-1})

[25] Figure 6 shows the estimation of the Eulerian correlation including only fast solar wind values. The means shown (black symbols) are for bins 0.2 wide. Again, the slope of the least squares linear fit is given in the upper left corner (0.80), and the slope is much smaller than those in Figures 2 and 4.

[26] The top panel of Figure 7 shows the Eulerian correlation function obtained from the fast solar wind single- and two-point correlation values. The means shown (black squares) are for 6 min wide bins, and the vertical bars are the errors of the means. For the fast solar wind, the decorrelation time is 114 ± 23 min, which is significantly shorter than the times found for the slow solar wind and for all solar wind speeds. Again, the lower panel of Figure 7 indicates the number of intervals that went into the determination of the Eulerian correlation function.

4. Discussion and Comparison With Theory

[27] It is well established that the fast solar wind and the slow solar wind differ in a number of ways. The fast wind, originating in coronal holes and found mainly at higher latitudes at solar minimum conditions, is hotter and less dense on average than the slow wind [*McComas et al*., 2000]. It has also been shown, both with single-spacecraft observations [*Dasso et al*., 2005] and two-spacecraft observations [*Weygand et al*., 2011], that the fast wind and slow wind differ in the dominant type of turbulent magnetic field fluctuations. Specifically, the fast wind contains a larger proportion of wave vectors oriented close to the direction of the mean magnetic field. Such fluctuations are often modeled as "slab" fluctuations. The fluctuations of the slow solar wind differ in having a larger proportion of the wave vectors perpendicular to the mean magnetic field direction and are represented by the quasi-two-dimensional turbulence model [*Goldstein et al*., 1994, 1995]. This reported difference in the dominant type of turbulence in fast and slow solar wind may help explain the above-described difference in Eulerian decorrelation times.

[28] The approximation that solar wind fluctuations are a superposition of these two pure symmetries is a matter of convenience in calculations but leads to reasonable agreement with cosmic ray scattering observations [*Bieber et al*., 1994] and direct observational tests of rotational symmetries [*Bieber et al*., 1996]. A more precise perspective is that such idealized models distinguish between fluctuations that are of the "quasi-slab" type with predominantly parallel wave vectors and a greater degree of Alfvén wave effects and "quasi-two-dimensional" fluctuations that lack significant wave signatures and remain at lower Alfvén wave frequencies. In fact, the domain of quasi-two-dimensional turbulence may be defined as the wave vector region in which the estimated nonlinear times are shorter than the estimated Alfvén time scales. Thus, in quasi-two-dimensional turbulence, dominant dynamical effects are nonlinear, and the role of the Alfvénic couplings is to limit the region of wave vector space where this nonlinear dominance may occur. This contrast between expected amounts of wavelike and nonlinear activity in different regions of the wave vector space provides the elementary basis for understanding how turbulence geometry influences Eulerian decorrelation.

[29] The connection between Eulerian decorrelation and underlying time scales of the turbulence is readily seen in the relation [*Zhou et al*., 2004; *Matthaeus et al*., 2010]

$$E(t) = \int d^3k\, S(\mathbf{k}) G(\mathbf{k}, t) \tag{1}$$

where $E(t)$ is the omnidirectional energy spectrum, $S(\mathbf{k})$ is the three-dimensional energy spectrum tensor, and $\Gamma(\mathbf{k},t)$ is the scale-dependent correlation function that describes how the correlations at wave vector $\mathbf{k}$ degenerate as time separation, t, increases.

[30] The scope of the physics embodied in equation (1) may be unraveled for homogeneous, time stationary turbulence and is discussed at length in the literature [*McComb*, 1990; *Edwards*, 1964; *Chen and Kraichnan*, 1989; *Zhou et al*., 2004]. To determine $E(t)$, one needs to know the model energy spectrum $S(\mathbf{k})$ at all scales (and directions). This includes the often-idealized inertial range, but it also includes the large energy-containing scales that are not expected to be self-similar. In fact, the spectrum at large scales $k < 1/L_c$, where L_c is the correlation scale, contains a significant fraction of the total turbulent energy and may not take on any particular or simple form. One therefore expects that the large scales make significant contribution to $E(t)$. Moreover, the expected structure of the scale-dependent time correlations $\Gamma(\mathbf{k},t)$ further amplifies the sensitivity of the functional form of $E(t)$ to the behavior of the long wavelength fluctuations. This conclusion is evident in the discussions of *Edwards* [1964], *McComb* [1990], Zhou *et al*. [2004], and *Servidio et al*. [2011].

[31] The time decorrelation at wave vector $\mathbf{k}$ may be written in a sufficiently general form as $\Gamma(\mathbf{k},t) = \Gamma^*(t/T(\mathbf{k}))$ for suitably chosen $T(\mathbf{k})$, which may be interpreted as the relaxation time at scale $1/k$. [*Zhou et al*., 2004]. Generally, we expect that $\Gamma \rightarrow 0$ for large t for any k. Therefore, Γ^* is a decreasing function at large argument. It is further reasonable to suppose that $T(\mathbf{k}) = T^*(\mathbf{k}_\perp, k_\parallel)$, where perpendicular and parallel refer to the magnetic field direction, when the

Table 1. Comparison of the Different Correlation Times Scales Found in the Work of *Shalchi* [2008] With Our Decorrelation Time Scales

Model	τ_c Slab (min) ~ Fast Solar Wind	τ_c Two-Dimensional (min) ~ Slow Solar Wind
Empirical result	114 ± 23	215 ± 43
Magnetostatic model	∞	∞
Undamped shear Alfvén waves L_{slab}/V_a	178	∞
Damping model of dyn. turbulence $L_{slab}/(\alpha\ V_a)$	178	42
Random sweeping model $L_{slab}/(\alpha\ V_a)$	211	42
NADT model (plasma wave effects) L_{slab}/V_a	170	No effect
NADT model (dyn. turbulence effects) $(1/\sqrt{2})(B_0/\Delta B_{2d})(L_{2d}/V_a)$	64	71
$T_c = T_0/2$ model as in text	175	250

mean magnetic field is the dominant preferred direction. For wavelike activity, $T^* \sim \cos(k_{\|}\ V_a\ t)$, where V_a is the Alfvén speed associated with the mean magnetic field. This cosine oscillation would be expected to be modulated by an envelope function that decreases with increasing $k_\perp$. In particular, inertial range slab or quasi-slab fluctuations are likely to be described by this type of decaying oscillation. Quasi-two-dimensional turbulence, on the other hand, lacks significant wave decorrelation and instead involves strong perpendicular nonlinear decorrelation. If this loss of correlation occurs mainly through couplings that are local in scale, then a reasonable estimate based on isotropic Kolmogorov inertial range scaling is $T^* \sim (L/Z)/(kL)^{2/3}$, or specifically for strongly anisotropic quasi-two-dimensional turbulence, $T^* \sim (L/Z)/(k_\perp\ L)^{2/3}$. Here Z is a measure of the total turbulence amplitude in speed units. Still another important physical process is embodied in the random sweeping model, in which time decorrelation occurs by advection of inertial range fluctuations in the large-scale flow, which contains most of the energy. For sweeping, $T^* \sim 1/(kZ)$, or for the anisotropic case, $T^* \sim 1/(k_\perp\ Z)$ (see the discussions by *Chen and Kraichnan*, [1989] and *Servidio et al*. [2011] for more detail). It is important to note that the time scales associated with these estimates of inertial range time decorrelation are generally faster than the large-scale eddy turnover time.

[32] Estimates of contributions to time decorrelation of the above types have been employed in varying degrees of complexity in models of "dynamical turbulence" effect on particle scattering [*Schlickeiser and Achatz*, 1993; *Bieber et al*., 1994]. For dynamical effects on parallel scattering, the Eulerian spectrum (Fourier transform of $E(t)$) becomes important because the power at the particle gyrofrequency can drive resonant interactions with particles. The proton gyrofrequency is usually around 1 Hz at 1 AU in the solar wind. Such relatively high-frequency power is well separated from the reciprocal eddy turnover time and therefore depends mainly on inertial range time decorrelation. More complete treatment of temporal effects is needed for models that include perpendicular charged particle scattering, which is sensitive to energy at long wavelengths. This need, at least in part, motivated the assembly of a composite theory [*Shalchi et al*., 2006] that includes time decorrelation at energy-containing scales and at inertial range scales. More recently, *Shalchi* [2008] constructed several explicit models for $E(t)$ by assuming a particular form for $S(\mathbf{k})$ and adopting alternative choices for $\Gamma(\mathbf{k},t)$.

[33] In principle, *Shalchi* [2008] provides a selection of model-dependent Eulerian correlations, against which the present observational results can be compared. To understand how these models might be compared to observations, it is essential to note that the large-scale fluctuations will almost always dominate the large time asymptotic behavior of the Eulerian correlation.

[34] Table 1 lists the six models compiled by *Shalchi* [2008], along with the dominant times scales, which are given both algebraically and numerically for nominal fast and slow solar wind conditions. These time scales are estimated based on observed correlation scales, interplanetary magnetic field and magnetic field fluctuations, and solar wind Alfvén speed. The estimate of the correlation-scale lengths we use are $1.3 \cdot 10^6$ and $1.7 \cdot 10^6$ km for the fast (slab turbulence) and slow (quasi-two-dimensional turbulence) solar wind, respectively. The values adopted are the average of the values shown in Table 1 of *Weygand et al*. [2011] over all solid angles relative to the mean magnetic field for each range of solar wind speed. The fast solar wind correlation scales range from $1.0 \cdot 10^6$ to $1.9 \cdot 10^6$ km, and the slow solar wind values spanned $1.1 \cdot 10^6$ to $2.8 \cdot 10^6$ km. The values of the nominal magnetic field, amplitude of the magnetic field fluctuations, and Alfvén speed used to calculate the decorrelation time scales in our Table 1 are 5 nT, 1 nT, and 85 km/s and 58 km/s for the Alfvén speeds in the fast and slow solar wind, respectively. These values were obtained using solar wind data from 2003 (arbitrarily selected).

[35] The explicit models of *Shalchi* [2008] may be compared with the present observational results. We estimated the normalized decorrelation times from Figures 1 and 3 of *Shalchi* [2008] and used empirical values of underlying parameters (Alfvén speed, etc.) to calculate the values provided in Table 1. For the damping model and the random sweeping model, an estimate of the turbulence parameter (α) is required. The parameter α, which may vary between 0 and 1, indicates the strength of the dynamical turbulence effects where a value of 0 corresponds to magnetostatic turbulence and $\alpha = 1$ corresponds to strongly dynamical turbulence. For simplicity, we have set α to 1, but we note that the decorrelation time can take values up to infinity depending on the selected α parameter (see Table 1). Table 1 demonstrates that none of the *Shalchi* [2008] models reproduce the values obtained from our empirical study. However, the models do produce decorrelation times within a factor of 3 of the empirical values. However, we note that the decorrelation times are sensitive to parameter values, as we discuss further below.

[36] In comparing the models to observations, it is important to recognize that the "correlation time scale" in the work of *Shalchi* [2008] refers to the long-time asymptotic decay time scale of the Eulerian correlation function and that this may or may not correspond to Eulerian

decorrelation. For example, the decorrelation time may be established at a shorter time for frequently encountered turbulence properties. On the other hand, if Eulerian decorrelation is dominated by the time variation of the largest energy-containing eddies, then these might control both Eulerian decorrelation and time-asymptotic decorrelation. As a practical matter, the decorrelation time is often estimated using the "1/e" value of the correlation function. If the long-time behavior of $E(t)$ is determined by the decorrelation of the large eddies, then the inertial range time decorrelation would influence mainly the intermediate time scale decorrelation. Generally, the models appropriate to the inertial range, such as the nonlinear model or the random sweeping model, are characterized by decorrelation at time scales faster than the energy-containing range as described above. Numerical experiments suggest that random sweeping is likely the dominant decorrelation effect in the inertial range (see *Servidio et al.*, [2011] for more details). In the present paper, we obtained an approximate time decorrelation using an exponential fit. Therefore, the simplest estimate for decay of the large energy-containing scales is appropriate, namely, the large-scale eddy turnover time $\tau_{eddy} = L/Z$. Here L is an appropriate correlation scale, and Z is the turbulence amplitude in speed units. Consequently, the differences in the "1/e" values of the Eulerian correlation models tabulated by *Shalchi* [2008] are likely not due to details of inertial range decorrelation but rather how decorrelation occurs in the large-scale energy-containing range. For example, the substantial difference between decorrelation in the nonlinear anisotropic dynamical turbulence (NADT) model and either the sweeping or nonlinear decay model of *Shalchi* [2008] can be traced mainly to the choice of parallel correlation scale $L_{\|}$. In particular, $L_{\|}$ is assumed by Shalchi [2008] to be 10 $L_{\perp}$. Such a choice is poorly motivated in observations, where a more accurate relationship would be $L_{\|} = 2\ L_{\perp}$.

[37] If we use the maximum correlation scales from Table 1 of *Weygand et al*. [2011], then the NADT model for slablike turbulence has a decorrelation time of ~95 min, which is within the uncertainty of our empirical value. Also, if we again use the maximum quasi-two-dimensional correlation scale and $\alpha = 0.3$, then the damping model and random sweeping model produce quasi-two-dimensional decorrelation times (~230 min) within the uncertainty of our empirical model, but the slab decorrelation times are much larger (>850 min) than our empirical values. However, there is no real justification for adjusting the input values other than to produce decorrelation times similar to our empirical model, and we cannot clearly say that one model is superior to another. The sensitivity of the models to correlation scales, other parameters (e.g., α), and other factors such as the assumed form of the energy spectrum suggests that a more simplified treatment is warranted.

[38] The relative effects of small-scale decorrelation and large-scale decorrelation on the Eulerian correlation function E(t) may be estimated in a very elementary model. Suppose that ΔB_0^2 is the energy in the energy-containing range at scales approximately ≥L and that the correlation time for the large structures is T_0. We treat the inertial range in a simple way that has energy ΔB_1^2 and a correlation time scale T_1. Assuming exponential time decorrelation in both ranges, $E(t) = \Delta B_0^2 \exp(-t/T_0) + \Delta B_1^2 \exp(-t/T_1)$, from which the correlation time (integral time scale) is

$$T_c = \left(\frac{\Delta B_0^2}{\Delta B^2}\right) T_0 + \left(\frac{\Delta B_1^2}{\Delta B^2}\right) T_1 \qquad (2)$$

[39] Thus, the overall correlation time is the energy-weighted average of the large-scale decorrelation time and the mean inertial range decorrelation time. For many simple models of turbulence spectra, the energy in the large scales is of the same order as the energy in the power law inertial range. Therefore, one might assume that the energy is apportioned equally, and $\Delta B_0^2/\Delta B^2 = ½$. This is a convenient and reasonable but arbitrary choice. In addition, the time scales may be ordered so that $T_1 << T_0$. This follows from the arguments above. From these simplifying assumptions, one obtains that $T_c = T_0/2$, and the global decorrelation time is just half the large-scale correlation time. From this formulation, we can use an estimate that $L_c = 10^6$ km and $Z = 33$ km/s (see *Breech et al*., [2008]) to find $T_0 = 500$ min. If half the energy is in the large scales, we conclude that $T_c \sim 250$ min (see last line of Table 1). This is remarkably close to the overall fit time scales in Figures 3 and 5, which are $T_c = 226 \pm 18$ min and 215 min ± 43 min, respectively.

[40] The results of this study were obtained from turbulent fluctuations observed in the magnetic field, and our discussion that addresses some of the theories associated with the Eulerian correlation function and decorrelation time has been more general. It is worth mentioning that the work of *Stawarz et al*. [2009] has shown that magnetic and velocity fluctuations show different scaling in the solar wind, and hence, including plasma data in the theoretical interpretations might be more complex than the concepts discussed here.

5. Conclusions

[41] Analysis of the solar wind intervals independent of the solar wind speed gave a decorrelation time of 226 ± 18 min, which is about 30% larger than the value of 174 min found by *Matthaeus et al*. [2010]. It is unclear if the difference is statistically significant since no uncertainty was given in the earlier study. We attribute the possible difference between the two results to the difference in the lengths of the solar wind intervals and the inclusion of additional solar wind spacecraft that provided intervals with small separations (measured by the THEMIS/ARTEMIS P1 and P2 spacecraft). Analysis of slow and fast solar wind intervals gave decorrelation times of 215 ± 43 min and 114 ± 23 min, respectively. The difference between the two values is statistically significant, and a discussion of a potential theoretical and observational basis for this difference seems appropriate. The previous section provided a brief digression into a discussion of the physics that controls Eulerian decorrelation.

[42] Theoretical and empirical estimates of decorrelation times are less familiar than estimates of the index of the energy spectrum but have equally important implications for understanding solar wind turbulence and making space weather predictions. Both time decorrelation and the turbulence amplitude strongly impose limits to prediction, while time decorrelation is responsible for departures from the frozen-in flow condition. Time decorrelation also influences particle scattering in several important ways. Under

some conditions, power in the time variations (measured by the Eulerian frequency spectrum) can control scattering through 90° pitch angles. This can have a strong or even controlling influence on parallel transport [*Bieber et al*., 1994] in much the same manner that the geometry of the turbulent fluctuations (e.g., two-dimensional vs. slab fluctuations [*Schlickeiser*, 2002]) influences the transport of energy. Time decorrelation is also critical because it enters explicitly into theories of perpendicular diffusion and magnetic field line random walk [*Matthaeus et al*., 2003; *Shalchi et al*., 2007].

[43] In the present study, we have found a significant linkage between the effects of time decorrelation and geometry in that the dominantly slablike fast wind also decorrelates faster in time than the quasi-two-dimensional slow solar wind. This could have interesting implications for particle transport, especially in the context of solar cycle dependence of the solar modulation of galactic cosmic rays [*George et al*., 2009]. A full discussion of these possible effects is beyond the scope of the present paper.

[44] Finally, the observed wind speed dependence of time decorrelation has immediate consequences. In investigations of the response of Earth's magnetosphere to the magnetic field of the solar wind, it is common to assume that the solar wind interplanetary magnetic field is frozen in and evolves little over relatively short distances such as from the L1 point to the Earth's magnetosphere when the propagation time is on the order of 30 to 60 min. This assumption is fundamental to space weather predictions and warnings. The decorrelation times here demonstrate that, on average, the assumption that the interplanetary magnetic field fluctuations are frozen in from the L1 point the Earth is valid, but over large distances compared with the Earth to L1 separation, the frozen-in assumption will break down first for the fast solar wind. Thus, the speed of the solar wind becomes an important factor in making predictions based on upstream measurements and should be more reliable when the solar wind speed is high.

[45] **Acknowledgments.** This work was supported by NASA grant NAG5-12131 and NSF SHINE grant AGS-1155841 at UCLA. W.H. Matthaeus is partially supported by NSF grant AGS-1063439 and the SHINE program, NASA NNX08AI47G and the Heliophysics theory program, and the Solar Probe Plus project at the University of Delaware. S. Dasso thanks the Argentinean grant UBACyT 20020090100264 (UBA). S. Dasso is a member of the Carrera del Investigador Científico (CONICET). We would like to thank M.L. Goldstein, Krishan K. Khurana, and Raymond J. Walker for their helpful discussions.

[46] Philippa Browning thanks Melvyn Goldstein and Zoltan Voeroes for their assistance in evaluating this paper.

References

Auster, H. U., et al. (2008), The THEMIS fluxgate magnetometer, *Space Sci. Rev.*, *141*, 235–264.

Bieber, J. W., W. Wanner, and W. H. Matthaeus (1996), Dominant two-dimensional solar wind turbulence with implications for cosmic ray transport, *J. Geophys. Res.*, *101*, 2511.

Bieber, J. W., W. H. Matthaeus, C. W. Smith, W. Wanner, M.-B. Kallenrode, and G. Wibberenz (1994), Proton and electron mean free paths: The Palmer consensus revisited, *Ap. J.*, *420*, 294.

Breech, B., W. H. Matthaeus, J. Minnie, J. W. Bieber, S. Oughton, C. W. Smith, and P. A. Isenberg (2008), Turbulence transport throughout the heliosphere, *J. Geophys. Res.*, *113*, A08105, doi:10.1029/2007JA012711.

Chen, S., and R. H. Kraichnan (1989), Sweeping decorrelation in isotropic turbulence, *Phys. Fluids A*, *1*, 2019.

Dasso, S., L. J. Milano, W. H. Matthaeus, and C. W. Smith (2005), Anisotropy in fast and slow solar wind fluctuations, *Astrophys. J.*, *635*, L181–L184.

Dasso, S, W. H. Matthaeus, J. M. Weygand, P. Chuychai, L. J. Milano, C. W. Smith, and M. G. Kivelson (2008), ACE/Wind multispacecraft analysis of the magnetic correlation in the solar wind, Proceedings of the 30th International Cosmic Ray Conference, vol. 1 (SH), pp. 625–628.

Edwards, S. F. (1964), The statistical dynamics of homogenous turbulence, *J. Fluid Mech.*, *18*, 239.

George, J. S., et al. (2009), Elemental Composition and Energy Spectra of Galactic Cosmic Rays During Solar Cycle 23, *Astrophys. J.*, *698*, 1666, doi:10.1088/0004-637X/698/2/1666.

Goldstein, M. L., D. A. Roberts, and C. A. Fitch (1994), Properties of the fluctuating magnetic helicity in the inertial and dissipation ranges of solar-wind turbulence, *J. Geophys. Res.*, *99*, 11,519.

Goldstein, M. L., D. A. Roberts, and W. H. Matthaeus (1995), Magnetohydrodynamic turbulence in the solar wind, *Ann Rev. Astron. Astrophys.*, *33*, 283.

Jokipii, J. R. (1973), Turbulence and Scintillations in the Interplanetary Plasma, *Ann. Rev. Astron. Astrophys.*, *10*, 1.

Kokubun, S., T. Yamamoto, M. H. Acuna, K. Hayashi, K. Shiokawa, and H. Kawano (1994), The Geotail magnetic field experiment, *J. Geomag. Geoelec.*, *46*, 7–21.

Lepping, R. P., et al. (1995), The Wind magnetic field investigation, *Space Sci. Rev.*, *71*, 207–229.

Matthaeus, W. H., G. Qin, J. W. Bieber, and G. P. Zank (2003), Nonlinear collisionless perpendicular diffusion of charged particles, *Astrophys. J.*, *590*, L53, doi:10.1086/376613.

Matthaeus, W. H., S. Dasso, J. M. Weygand, M. G. Kivelson, and K. T. Osman (2010), Eulerian Decorrelation of Fluctuations in the Interplanetary Magnetic Field, *Astrophys. J. Lett.*, *721*, L10–L13, doi:10.1088/2041-8205/721/1/L10.

McComas, D. J., B. L. Barraclough, H. O. Funsten, J. T. Gosling, E. Santiago-Munoz, R. M. Skoug, B. E. Goldstein, M. Neugebauer, P. Riley, and A. Balogh (2000), Solar wind observations over Ulysses' first full polar orbit, *J. Geophys. Res.*, *105*, 10,419–10,433.

McComb, W. D. (1990), *The Physics of Fluid Turbulence*, Oxford University Press, New York.

Montgomery, D. C. (1982), Major disruptions, inverse cascades, and the Strauss equations, *Phys. Scr.*, *T2*(1), 83–88.

McFadden, J. P., C. W. Carlson, D. Larson, M. Ludham, R. Abiad, B. Elliott, P. Turin, M. Marckwordt, and V. Angelopoulos (2008), The THEMIS, ESA plasma instrument and In-flight Calibration, *Space Sci. Rev.*, *141*, 277–302.

Nozdrachev, M. N., et al. (1995), Magnetic field measurements onboard the INTERBALL TAIL spacecraft: the FM-3I instrument, INTERBALL. Mission and Payload, CNES-IKI-RSA, 228–229.

Paularena, K. I., J. D. Richardson, G. N. Zastenker, and P. A. Dalin (1999), Solar wind correlations: Statistical and case studies, *Proceedings of the Ninth International Solar Wind Conference*, *Nantucket*, *MA*, S.R. Habbal, R. Esser, J. V. Hollweb, P. A. Isenberg eds., 585–588, AIP Conference Proceedings 471.

Ridley, A. J. (2000), Estimations of the uncertainty in timing the relationship between magnetospheric and solar wind processes, *J. Atmos. Sol.-Terr. Phys.*, *62*, 757.

Ruiz, M. E., S. Dasso, W. H. Matthaeus, E. Marsch, and J. M. Weygand (2011), Aging of anisotropy of solar wind magnetic fluctuations in the inner heliosphere, *J. Geophys. Res.*, *116*, A10102, doi:10.1029/2011JA016697.

Schlickeiser, R., and U. Achatz (1993), Cosmic-ray particle transport in weakly turbulent plasmas. I. Theory, *J. Plasma Phys.*, *49*, 63.

Schlickeiser, R. (2002), *Cosmic ray astrophysics, Astronomy and Astrophysics Library, Physics and Astronomy Online Library*, Springer, Berlin.

Servidio, S., V. Carbone, P. Dmitruk, and W. H. Matthaeus (2011), Time decorrelation in isotropic magnetohydrodynamic turbulence, *EPL*, *96*, 55003, doi:10.1209/0295/96/55003.

Shalchi, A., J. W. Bieber, W. H. Matthaeus, and R. Schlickeiser, (2006), Parallel and perpendicular transport of heliospheric cosmic rays in an improved dynamical turbulence model, *Astrophys. J.*, *642*, 230.

Shalchi, A., R. C. Tautz, and R. Schlickeiser (2007), Field line wandering and perpendicular scattering of charged particles in Alfvénic slab turbulence, *Astron. Astrophys.*, *475*, 415–420, doi:10.1051/0004-6361:20078030.

Shalchi, A. (2008), Forms of Eulerian correlation functions in the solar wind, *Astrophys. Space Sci.*, *318*, 149–159, doi:10.1007/s10509-008-9932-2.

Smith, C. W., J. L. Heureux, N. F. Ness, M. H. Acuna, L. F. Burlaga, and J. Scheiffele (1998), The ACE magnetic fields experiment, *Space Sci. Rev.*, *86*, 613–632.

Stawarz, J. E., C. W. Smith, B. J. Vasquez, M. A. Forman, and B. T. MacBride (2009), The turbulent cascade and proton heating in the solar wind at 1 AU, *Astrophys J.*, *697*, 1119–1127.

Taylor, G. I. (1938), The spectrum of turbulence, *Proc. Roy. Soc.*, *164*, 476–490.
Weygand, J. M., W. H. Matthaeus, S. Dasso, and M. G. Kivelson (2011), Correlation and taylor scale variability in the interplanetary magnetic field fluctuations as a function of solar Wind Speed, *J. Geophys. Res.*, *116*, A08102, doi:10.1029/2011JA016621.
Zank, G. P., and W. H. Matthaeus (1992), Waves and turbulence in the solar wind, *J. Geophys. Res.*, *97*, 17,189.
Zhou, Y., W. H. Matthaeus, and P. Dmitruk (2004), Magnetohydrodynamic turbulence and time scales in astrophysical and space plasmas, *Rev. Mod. Phys.*, *76*, 1015.